Electronic Supplementary Material (ESI) for Chemical Communications.
This journal is © The Royal Society of Chemistry 2023

Supporting Information

Improved Photocatalytic Activity of TiO_2 with Regulated Covalent Organic Framework Thin Film

Xiaochi Han†[a], Wenbo Dong†[b], Longyu Li[b], Xuemei Zhou*[a]*

[a]School of Chemical Engineering, Sichuan University, Chengdu 610065, P. R. China, E-mail: xuemeizhou@scu.edu.cn;

[b]College of Polymer Science and Engineering, State Key Laboratory of Polymer Materials Engineering, Sichuan University, Chengdu, 610065, P. R. China, E-mail: longyu88@scu.edu.cn.

†These authors contributed equally to the work.

Experimental section

1. Chemicals

If not stated otherwise, all reagents were purchased from commercial sources and used without any further purification. 1,3,5-tris (p-formylstyryl) benzene was synthesized adapt to a procedure reported by our group.[1] Tetrahydrofuran (99.5%), mesitylene (99%), dioxane (99%), methanol (99%), acetone (99%), acetic acid (99%), p-phenylenediamine (98%), and sulphuric acid (H_2SO_4, 98%) were purchased from Adamas-beta Co., China. Toluene (99.5 %) and hydrofluoric acid (HF, 98%) were purchased from Chengdu Kelong Chemical Co., China. Chloroplatinic acid hexahydrate ($H_2PtCl_6 \cdot H_2O$, ACS reagent) was purchased from SLGMA-ALDRICH Co., China. KH550 (98%) was purchased from GENERAL-REAGENT Co., China. Ti metal (thickness 0.1 mm, 99.99%) was purchased from ARITER.

2. Synthesis procedures

In brief, the TiO_2 NTAs were synthesized by anodizing a piece of Ti foil in a H_2SO_4/HF aqueous electrolyte under an applied voltage of 20 V.[2] Afterwards, TiO_2 NTAs were crystallized, followed by reflux with silane-based linker molecules (KH550, 3-aminopropyltriethoxysilane) in toluene to form self-assembled monolayers (SAMs).[3] Then, the coated TiO_2 NTAs were placed in the reaction tube during COF synthesis, where it is assumed that -CHO groups from the TFSB play dual roles: reacting with PDA to form the framework of the COF, with the -NH2 group of KH550 on the surface to anchor the COF film, both via imine condensation reactions. The thickness of the COF film was controlled by the loading of monomers in the reaction solution and the as-synthesized samples are denoted as COF/TiO_2-H, COF/TiO_2-M and COF/TiO_2-L from high to low concentrations (see **Table S1**).

2.1. Preparation of TiO_2 NTAs

For the fabrication of TiO_2 NTAs, titanium foils were cut into pieces (1.5 cm×1.5 cm) and cleaned by acetone, deionized water and ethanol, respectively. It took 10 min for each step in ultrasonic bath and dried using nitrogen stream. The anodization of Ti foil was performed at room temperature in a two-electrode electrochemical cell in which a Pt sheet and a Ti foil were used as the cathode and anode, respectively. The anodization was carried out at a constant voltage of 20 V for 5 h in 1M H_2SO_4 with 0.125 wt% HF. After anodization, the sample was cleaned with DI water and annealed at 450 °C for 1 h in air.

2.2 KH550 modification of TiO_2 NTAs

TiO_2 NTAs were welded to titanium wire and placed in a 50 mL three-neck flask. 5 μL KH550 was added in 30 mL toluene and the treatment was carried out at 110 ℃ for 24 hours. Afterwards the samples were washed with ethanol and dried in vacuum at 80 ℃ for 12 h.

2.3 Synthesis of COF

The COF powders were synthesized adopted a method from our previous work.[1] In brief, 1,3,5-tris (p-formylstyryl) benzene and p-phenylenediamine were added into a glass tube, then the mixture weas dissolved in mesitylene (0.5 mL) and dioxane (0.5 mL). 0.1 mL (6 M) aqueous HOAc aqueous solution was added to the mixture. Then the tube was flash frozen in a liquid nitrogen bath and degassed through three freeze-pump-thaw cycles and sealed under vacuum. Upon warming, the ampoule was placed in an oven at 120 ℃ and left undisturbed for 3 days. The resulting precipitate was filtered, and washed thoroughly by THF. The solid powder was dried and then subjected to Soxhlet extractions with THF and acetone for 1 day to remove the trapped guest molecules. The solid powder was washed by methanol for 12 h and then dried in supercritical CO_2. The powder was collected and dried under vacuum condition at 120 °C for 12 h to yield COF as a yellow powder.

2.4 Synthesis of COF/TiO_2

The preparation of COF/TiO_2 was modified with the procedure of COF synthesis. Following the addition of HOAc aqueous solution, the TiO_2 NTAs films were added into the mixture. With the same procedure of heating in an oven at 120 ºC for 3 days, the resulting TiO_2 NTAs with COF loading were transferred into THF, acetone and methanol for 1 day to remove the trapped guest molecules. Finally, the COF/TiO_2 samples were taken out of methanol and dried. By adjusting the dosage of 1,3,5-tris (p-formylstyryl) benzene and p-phenylenediamine in equal proportion, COF/TiO_2-H, COF/TiO_2-M, and COF/TiO_2-L from high to low COF loading were obtained. The concentration ratios are shown in **Table S1.**

Table S1. COF monomer concentration used during synthesis in details.

Samples	1,3.5-tris (p-formylstyryl) benzene			P-phenylenediamine		
	m/mg	n/mmol	Eq.	m/mg	n/mmol	Eq.
COF/ TiO_2-H	5.85	0.0125	1	2.025	0.01875	1.5
COF/ TiO_2-M	2.925	0.00625	1	1.0125	0.009375	1.5
COF/ TiO_2-L	1.75	0.0025	1	0.405	0.00375	1.5

3. Characterization

3.1 SEM

The morphology of samples was characterized using a JEOL JSM-6700 scanning electron microscope (SEM) and the samples were fixed on a flat copper sample holder.

3.2 TEM

TEM and high-resolution transmission electron microscopy (HRTEM) were acquired usign a Japan JEOL-F200 TEM at an acceleration voltage of 200 kV. The sample was taken from the Ti substrate and dispersed in ethanol. 20 μL suspension was dropped on an ultra-thin carbon film supported by 300 mesh copper TEM grid and

dried.

3.3 XRD

X-ray diffraction (XRD) patterns were recorded on an EMPYREAN instrument equipped with Cu, Kα1 = 1.540598, Kα2 = 1.544426 in the 2θ range of 2°– 80° with a step size of 0.01°.

3.4 Raman

Raman spectroscopy was performed on a Thermal Fisher DXR Raman spectrometer using an incident laser at 455 nm.

3.5 XPS

X-ray photoelectron spectroscopy (XPS) was performed by PHI 5000 VersaProbe III with a monochromatic Al Kα X-ray source with the beam size of 100 μm. Charge compensation was achieved by the dual beam charge neutralization and the binding energy was corrected by setting the binding energy of the Ti 2*p* at 458.8 eV. And in-situ irradiated XPS was carried out under a 5W LED light source at 365 nm.

3.6 PL

The photoluminescence (PL) and Time-resolved photoluminescence (TRPL) measurement spectra were recorded on laser flash spectrometer (Edinburgh Instruments FLS1000) at room temperature. PL test was performed with an excitation light source at 340 nm. TRPL was measured at excitation of 375 nm and the decay of PL intensity was monitored at 420 nm.

3.7 TGA

The thermo-gravimetric analysis (TGA) from 40-800 ℃ was carried out on a NETZSCH TG209F3 in a nitrogen atmosphere using a 10 ℃/min ramp without equilibration delay.

3.8 Electrochemical measurement

The photocurrent density, transient photocurrent response, electrochemical impedance spectra (EIS), and Mott Schottky plot were measured via a PGSTAT204A electrochemical station in a standard three electrode configuration. The working electrode was COF/TiO_2 samples. A Pt electrode and an Ag/AgCl electrode serve as counter electrode and reference electrode, respectively. 0.1 M Na_2SO_4 aqueous solution was used as electrolyte.

The carrier density was calculated from Mott Schottky sepctra by the following equation:[4, 5]

$$\frac{1}{C^2} = \frac{2}{N_D q \varepsilon_0 \varepsilon}\left(U - U_{FB} - \frac{kT}{q}\right)$$

where C is the space charge capacitance in the semiconductor, N_D is the carriers concentration (for n-type semiconductors), q is the elemental charge value (1.6×10^{-19} C), ε_0 is the permittivity of a vacuum (8.86×10^{-12} F m^{-1}), ε is the relative permittivity of anatase TiO_2(48), U is the applied potential, U_{FB} is the flat band potential, T is the temperature, and k is the Boltzmann constant.

The Mott Schottky method was used to quantitatively describe semiconductor junction as follows:

$$W = \left[\frac{2}{q\varepsilon\varepsilon_0 N_D}\left(U_s - \frac{kT}{q}\right)\right]^{1/2}$$

where W is the width of the space charge (depletion) layer due to contact, i.e., the energy band bending width. U_s is the induced surface potential barrier in a semiconductor.

The photocurrent density and transient photocurrent response were measured at a bias voltage of 0.5V vs. Ag/AgCl, and transient photocurrent response was recorded at six periodic on-off cycles under 340nm. EIS was collected with a frequency range of 0.01 Hz to 100000 Hz at a bias voltage of 1V vs. Ag/AgCl. The IPCE is obtained from the short-circuit photocurrent ($J_{shortcircuit}$) monitored at different excitation wavelengths (λ) with the following expression:[6]

$$IPCE(\%) = \frac{1240 \times J_{shortcircuit}\left(A/cm^2\right)}{\lambda \times I_{incident}\left(W/cm^2\right)} \times 100$$

Where the incident light wavelengths are selected in the range of 300-500nm, the

incident light intensity ($I_{incident}$) was measured by the light intensity meter (CEL-NP2000) in this range, and the $J_{shortcircuit}$ was obtained from the photocurrent density of the response.

3.9 BET

The surface area and porosity were investigated by nitrogen adsorption and desorption at 77 K using iPore400 (PhysiChem Instruments Lid.). The porosity analysis was obtained by analyzing the adsorption using non-local density functional theory (NLDFT).

3.10 Work Function Simulations

We have employed the DMol3 to perform the calculation of the work function of COF within the generalized gradient approximation (GGA) using the Perdew-Burke-Ernzerhof (PBE) formulation. The work function was calculated to be 3.563 eV.

4. Photocatalytic activity measurements

The COF/ TiO_2 was placed in a 40 mL photoreactor using a titanium wire. 300 μL 5 mM chloroplatinic acid was added in 4 mL water/ethanol (4:1=v:v) mixture. Pt (1.5 wt.%) was deposited on the sample using a side-illuminated 300W Xe lamp (wavelength range, 320 nm ≤ λ ≤ 780 nm) as the light source for 1 h. After deposition, the sample was placed into 20 mL water/ethanol (v:v=4:1). After reaction for 5 hours, 1 mL of gas was taken and fed into gas chromatography (FULI GC9790II) for analysis, and the GC is equipped with a thermal conductive detector (TCD), 5A Molecular Sieve column, using Argon (99.999%) gas as carrier gas.

To conduct the photocatalytic CO_2 reduction reaction, a glass reactor (volume: 350 mL) with a quartz window at the top and a 300W Xe lamp were employed. CO_2 was generated in situ by reacting 50 mL $NaHCO_3$ (1.28g, 0.015mol) aqueous solution with HCl (13 mL, 1M). The sample was placed on a ceramic plate and the reaction occurs under a pressure of about 50 kPa for 5 h. The sampling was performed at 1 h intervals with automatic injection of 1 μL gas mixture. The sampled gas was detected by gas

chromatography (Shimadzu GC-2030, Shimadzu instrument, Japan) equipped with a BarrierDischarge ionization detector (BID).

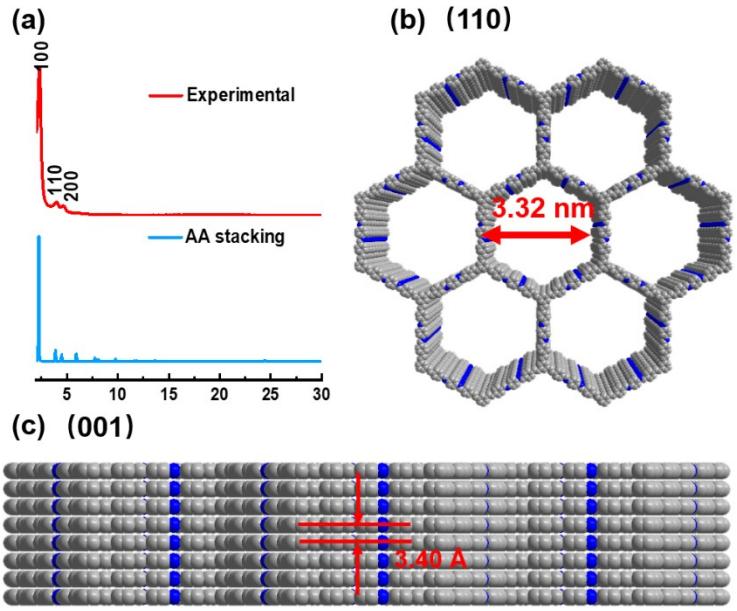

Fig. S1 (a) PXRD patterns of COF in experiment and in simulation. (b) Top view and (c) side view of the simulated reconstructed COF crystal structure.

The crystal structure of COF powders is demonstrated by powder X-ray diffraction (PXRD) patterns (**Fig. S1a**, top row), which exhibits a highly crystalline structure and agrees well with the simulated spectrum with an AA stacking model (**Fig. S1a**, bottom row). The strongest peak at 2.31° is corresponding to (100) facet and the diffraction peaks at 3.95°, 4.56°, 6.00°, and 26.18° are attributed to (110), (200), (210), and (001) facets, respectively. The modeling configuration exhibits a pore size of 3.32 nm and layer spacing of 3.40 Å (**Fig. S1b-c**), that is consistent with the pore size (3.32 nm) measured using N_2 adsorption-desorption isotherms. In addition, the COF powders show a large specific surface of 754.3 m^2/g.

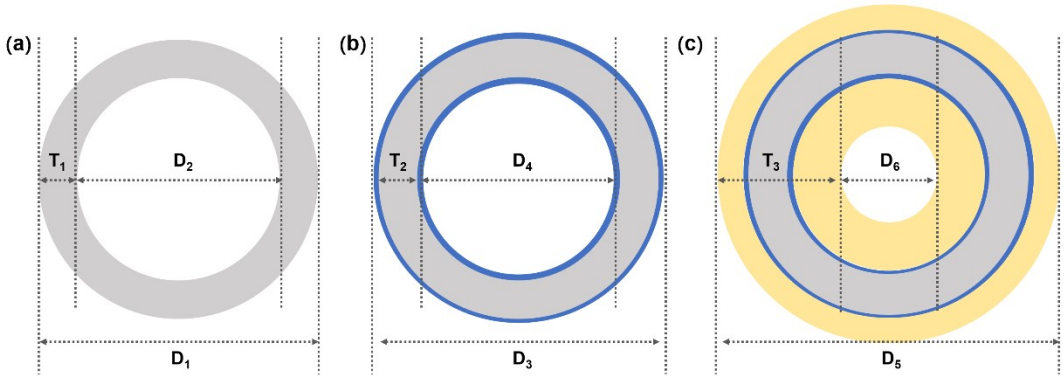

Fig. S2 Schematic diagram of tube diameter and thickness statistics calculation of TiO_2, KH550/TiO_2, and COF/TiO_2.

Fig. S2 shows the schematic diagram of tube diameter and thickness estimation, where D_1-D_6 are from SEM and TEM measurements, referring to the following:

D_1 - outer diameter of TiO_2 nanotubes.

D_2 - inner diameter of TiO_2 nanotubes.

D_3 - outer diameter of amine-modified nanotubes.

D_4 - inner diameter of amine-modified nanotubes.

D_5 - outer diameter of nanotubes after loading COF.

D_6 - inner diameter of nanotubes after loading COF, respectively.

The formula for calculating the tube thickness is as follows:

$$T_1 = \frac{1}{2}(D_1 - D_2)$$

$$T_2 = \frac{1}{2}(D_3 - D_4)$$

$$T_3 = \frac{1}{2}(D_5 - D_6)$$

$$T_{COF} = T_3 - T_2$$

where T_1 is the TiO_2 nanotube thickness, T_2 is the nanotube thickness after amine modification, T_3 is the nanotube thickness after COF loading, T_{COF} is the COF layer thickness.

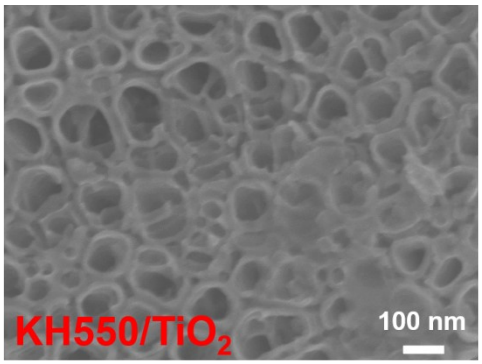

Fig. S3 SEM image of KH550/ TiO_2. Statistically, the diameter and wall thickness of KH550/ TiO_2 are 125 nm and 22 nm, respectively.

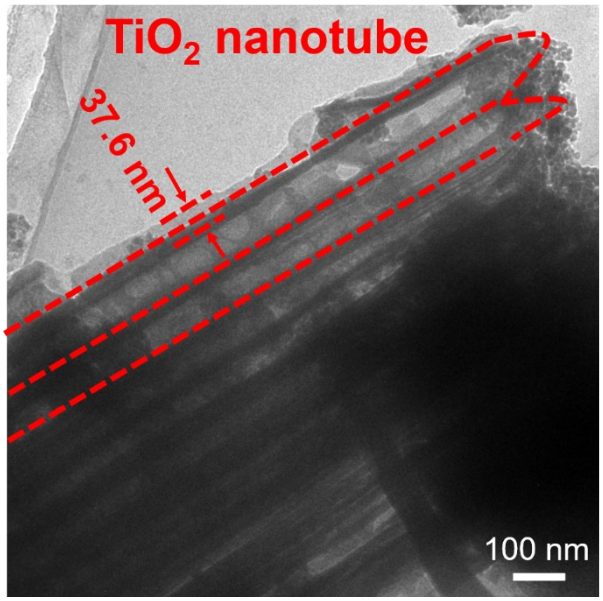

Fig. S4 TEM images of COF/TiO_2-M.

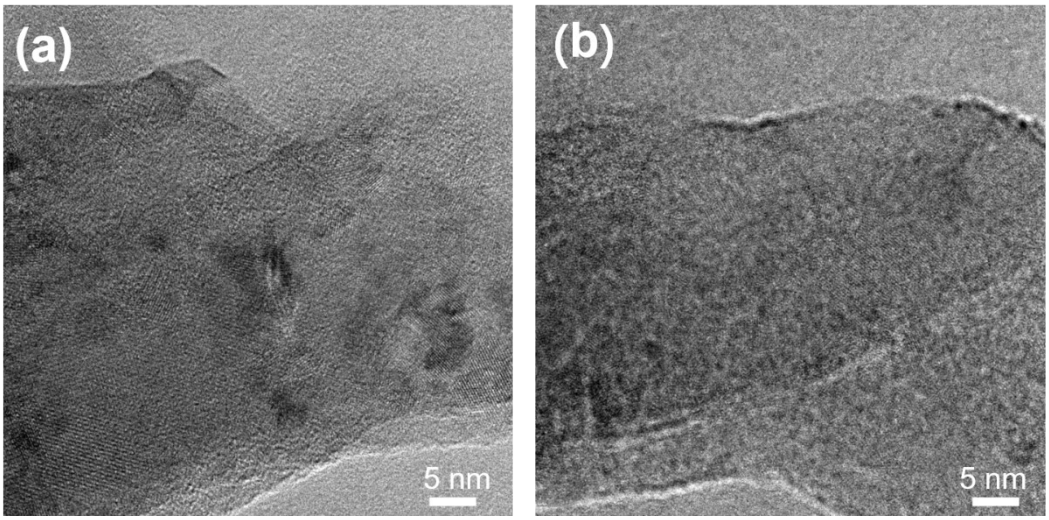

Fig. S5 HRTEM images of COF/TiO_2-H.

Table S2. Analysis on the diameter of top mouth and thickness of walls for TiO_2 NTAs at different synthetic stage from SEM. σ represents the standard deviation.

Samples	Diameter /nm	σ	Thickness /nm	σ	COF thickness/nm	σ
TiO_2 NTAs	114.4	19.6	16.6	5.0		
KH550/ TiO_2	124.6	19.2	22.1	5.8		
COF/ TiO_2-L	143.4	13.4	28.7	3.2	6.6	3.2
COF/ TiO_2-M	154.2	14.4	37.6	5.3	15.3	5.3
COF/ TiO_2-H	157.6	15.9	42.3	3.5	20.2	3.6

Table S3. Analysis on the tube diameter and thickness from TEM.

Samples	Diameter/nm	σ	Thickness/nm	σ	COF thickness/nm	σ
COF/ TiO_2-L	142.9	4.7	28.7	2.5	6.5	0.3
COF/ TiO_2-M	154.3	4.9	37.4	1.6	15.3	0.5
COF/ TiO_2-H	157.3	1.5	42.4	3.0	20.3	0.8

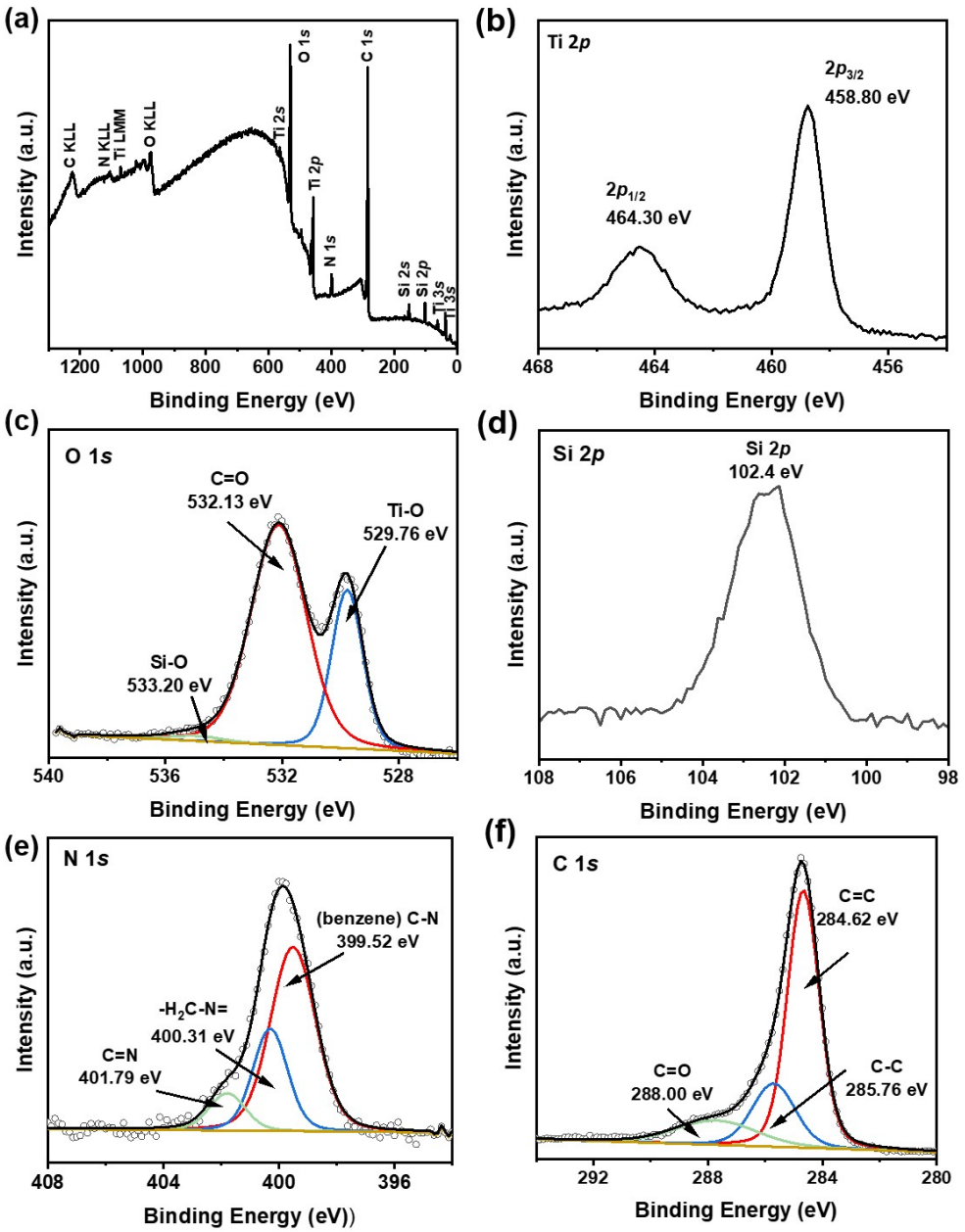

Fig. S6 (a) XPS survey spectrum of COF/TiO_2-M. and corresponding high resolution XPS spectra: (b) Ti 2*p*, (c) O 1*s*, (d) Si 2*p*, (e) N 1*s*, and (f) C 1*s*.

The XPS survey spectrum for COF/TiO_2-M further reveals the presence of Ti, O, Si, N, and C on the surface (**Fig. S6a**). The O 1*s* spectrum (**Fig. S6c**) presents three peaks with binding energies at 529.76, 532.13 and 533.20 eV, which are ascribed to oxygen in Ti-O, C=O, and Si-O from TiO_2, COF, and KH550, respectively. The N 1*s* spectrum can be deconvoluted into three peaks (**Fig. S6e**). Two peaks at 399.52 and 401.79 eV are attributed to (benzene) C-N and C=N in the COF imine structure,

respectively. Another peak appearing at 400.31 eV is assigned to the -H_2C-N= structure, which is a specific structure derived from the Schiff base reaction of the -NH_2 group of KH550 on TiO_2 with -CHO group of the COFs, suggesting chemical bonds between TiO_2 and the COFs. The C 1*s* spectrum (**Fig. S6f**) is deconvoluted into peaks at 284.62, 285.76, and 288.00 eV, which are identified to be C=C, C-C, and C=O bonds in the COF. The atomic ratio of these elements is compared to the theoretical ratios in the COF and KH550 (**Table S4 and S5**), suggesting that nitrogen and carbon are introduced by the COF film on the surface of the TiO_2 NTAs.

Table S4. Atomic concentrations of each element for COF/TiO_2-M from XPS measurement.

	C 1*s*	N 1*s*	O 1*s*	Si 2*p*	Ti 2*p*
RSF	0.314	0.499	0.733	0.368	2.077
Corrected RSF	21.068	33.303	48.296	55.688	236.374
Atomic content	63.16	3.91	25.25	3.56	4.12

Table S5. Comparison of theoretical atomic ratio from formula and experimental atomic ratio from XPS measurement.

atomic ratio		Si/O	Si/N	Si/C	N/C
experiment		0.141	0.910	0.056	0.062
theoretical	COF	---	---	---	0.051
	KH550	0.333	1	0.111	0.111

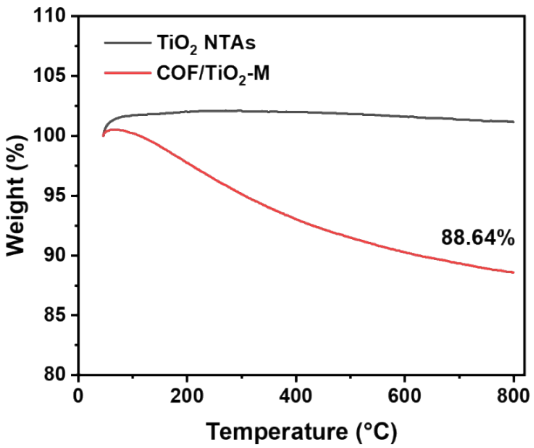

Fig. S7 TGA curves of TiO_2 and COF/TiO_2-M.

For COF/TiO_2-M, the maximum COF is 1.50 mg considering a 100% loading efficiency during COF synthesis. The thermo-gravimetric analysis (TGA) demonstrates that COF/TiO_2-M shows a weight loss of 11.36% at 800 °C, but TiO_2 has no weight loss (**Fig. S7**). Considering the mass of COF/TiO_2-M is 10.2 mg (determined by the average mass of several samples), the mass of COF is thus calculated to be 1.16 mg.

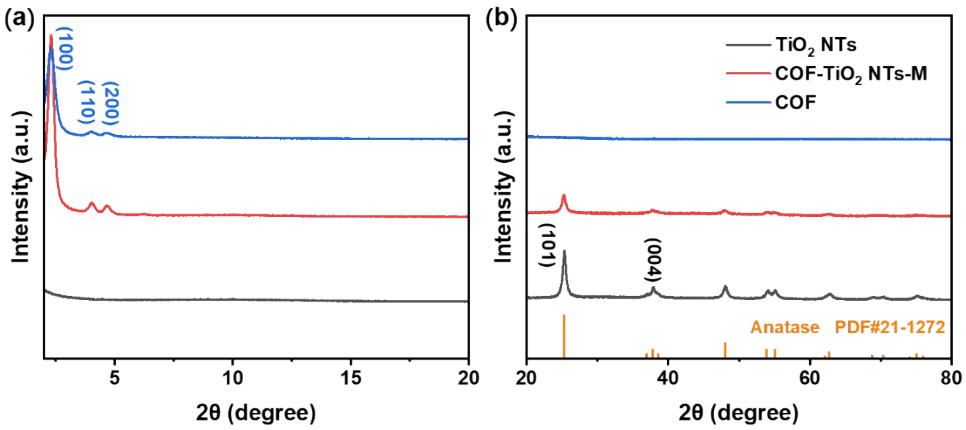

Fig. S8 XRD patterns of TiO_2 NTs powder, COF/TiO_2 NTs-M powder, and COF powder.

We have prepared anodic TiO_2 nanotube (TiO_2 NTs) powders using similar anodization conditions and used these powders to coat with COF. The mass ratio of TiO_2 NTs powder to COF is determined to be 1:2 during COF loading experiment, that is close to the estimated mass ratio of COF/TiO_2-M.

The XRD peaks of COF at 2.31°, 3.95°, 4.56° are assigned to the (100), (110), (200) facet of a primitive hexagonal lattice. Diffraction patterns for TiO_2 NTs powders at 25.27° and 37.80° are corresponding to the (101) and (004) plane of TiO_2 (PDF No. 21-1272).[7] XRD patterns of COF/TiO_2 NTs-M powders show the diffraction peaks of COF and TiO_2, suggesting the successful loading of COF.

The loading of COF on TiO_2 NTs powders results in a slight increase in surface area to 785.2 m^2 g^{-1} (**Fig. S9**).

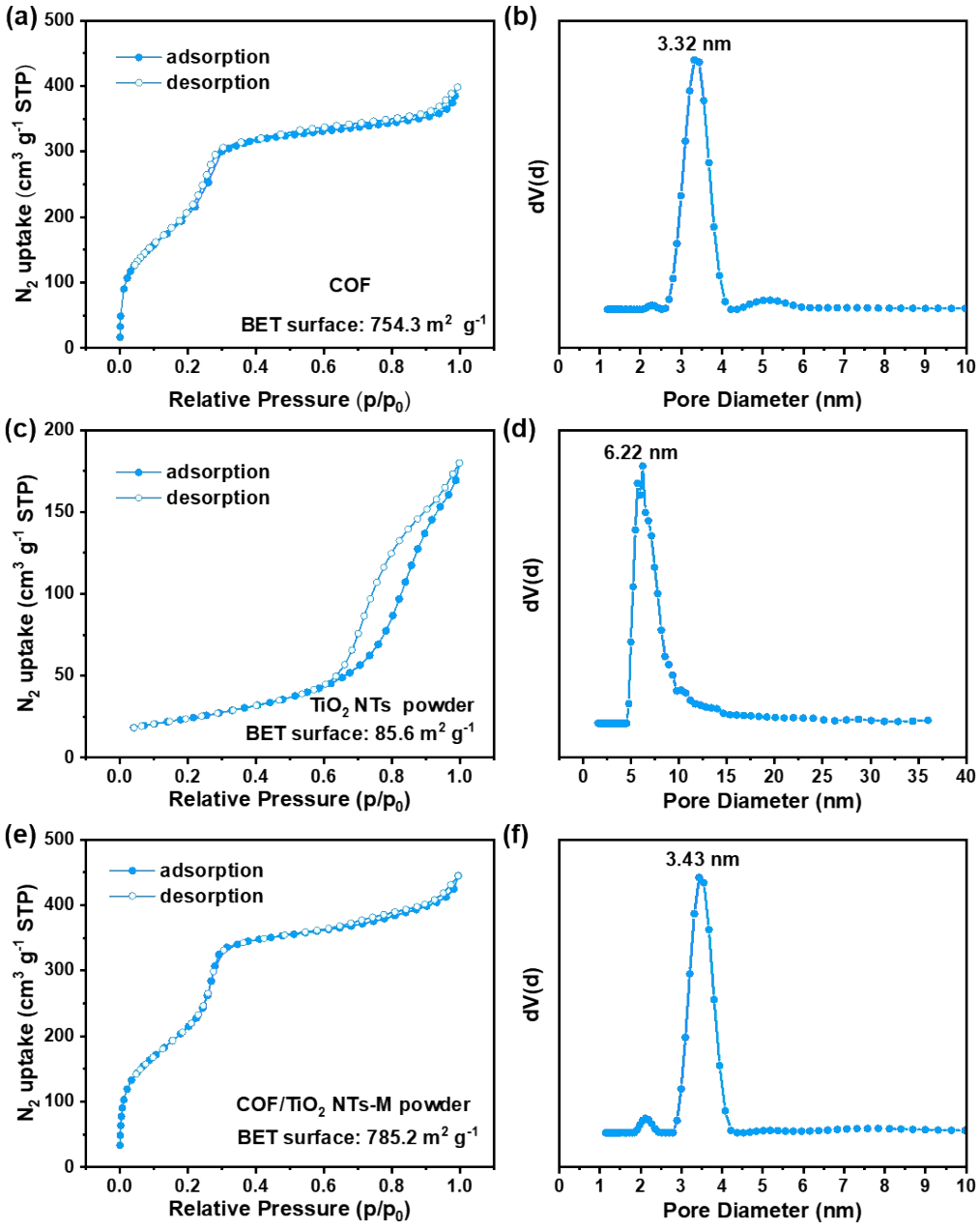

Fig. S9 Nitrogen adsorption-desorption isotherms and pore size distribution of (a-b) COF powder, (c-d) TiO_2 NTs powder and (e-f) COF/TiO_2 NTs-M powder.

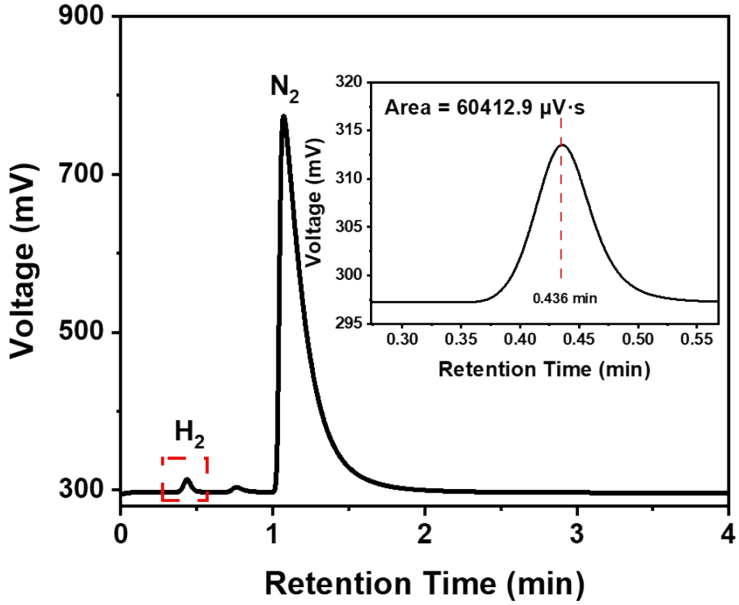

Fig. S10 Chromatogram of the highest H_2 yield of COF/TiO_2-M.

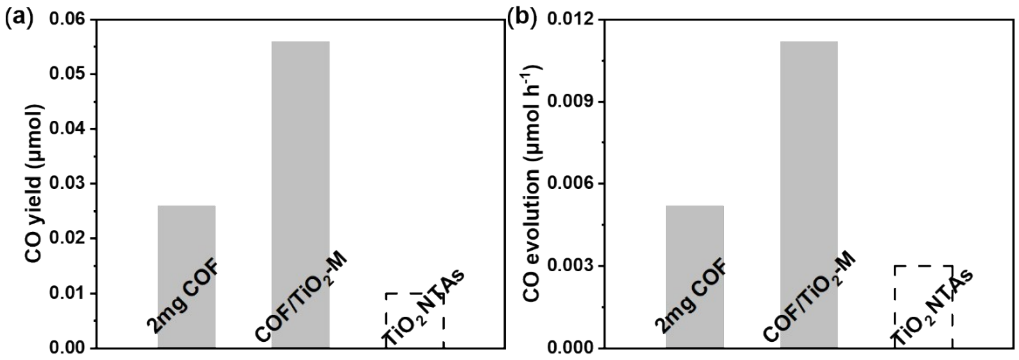

Fig. S11 (a) CO yield and (b) CO evolution of COF/TiO_2-M, COF, and TiO_2 for CO_2 reduction (dash line indicates 0).

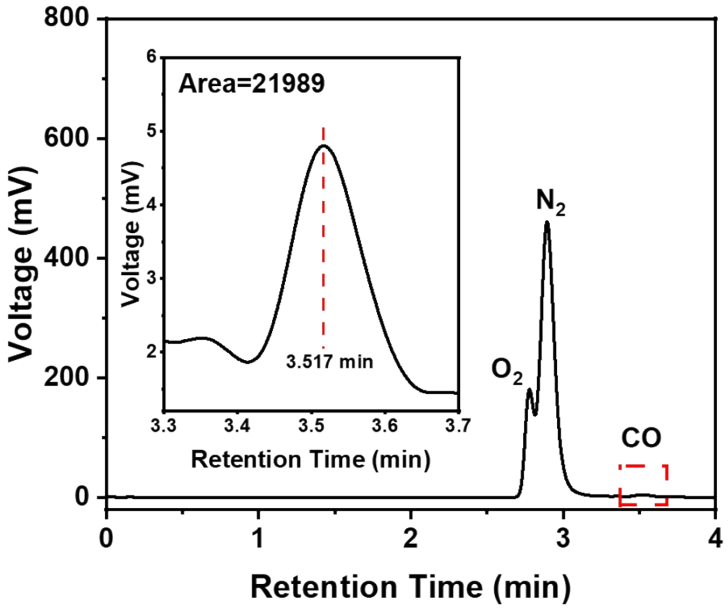

Fig. S12 Chromatogram of CO yield of COF/TiO_2-M.

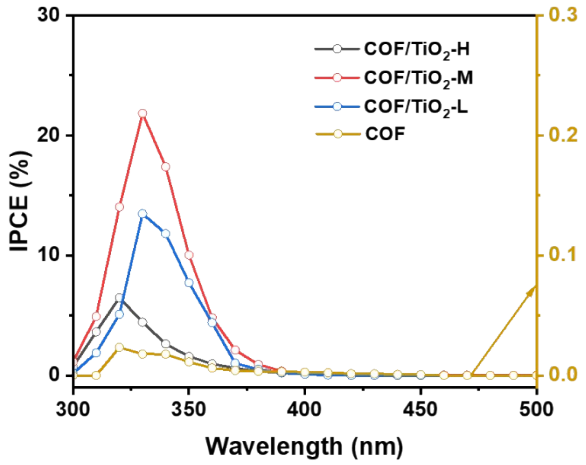

Fig. S13 IPCE of COF/TiO_2-H, COF/TiO_2-M, COF/TiO_2-L, and COF. **Fig. S13** exhibits the incident photon conversion efficiency (IPCE) as a function of excitation wavelength. COF/TiO_2-M is calculated to show the highest IPCE value, which agrees with the H_2 evolution results.

Table S6. The parameters used to fit the EIS of samples. The Nyquist plot is shown in **Fig. 3e**.

	R_{ct}/kΩ	R_s/Ω	CPE		χ^2
			Y_0	N	
COF/TiO_2-H	26.2	105.4	1.3×10^{-4}	0.94	0.0060
COF/TiO_2-M	13.1	107.2	1.3×10^{-4}	0.94	0.0065
COF/TiO_2-L	25.8	142.3	1.3×10^{-4}	0.93	0.0054
TiO_2 NTAs	35.1	154.0	1.4×10^{-4}	0.93	0.0241
COF	47.7	73.2	1.3×10^{-4}	0.91	0.0834

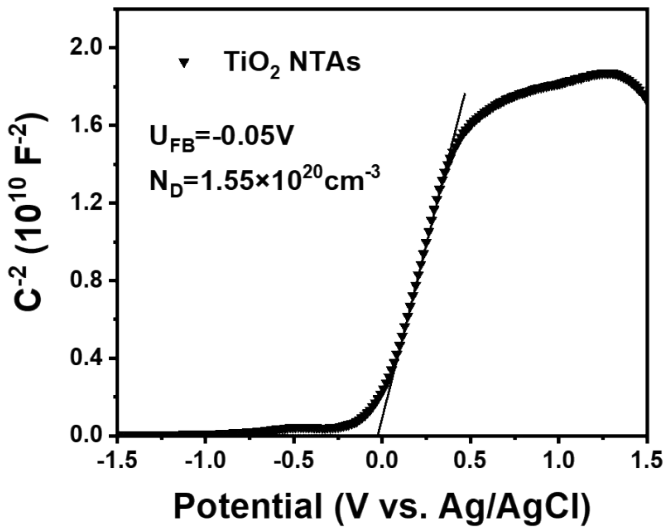

Fig. S14 Mott–Schottky plots of TiO_2.

Table S7. Summary of the fitting parameters of TRPL from **Fig. 4b**.

Catalyst	Fitting Parameters					
		Value (ns)		Value		Value
TiO_2 NTAs	τ_1	0.55	A_1	1260.76	τ_{ave} *(ns)*	1.41
	τ_2	4.47	A_2	43.61	$\chi 2$	1.039
COF/TiO_2 -M	τ_1	0.79	A_1	937.24	τ_{ave} *(ns)*	1.88
	τ_2	3.19	A_2	191.91	$\chi 2$	1.070

The equation used to fit the spectra is shown as below:

$$R(t) = \Sigma A_i e^{-\frac{(t)}{(\tau_i)}} \quad (i = 1, 2)$$

And the average lifetimes are calculated as below:

$$\tau_{ave} = \frac{\Sigma A_i \tau_i^2}{\Sigma A_i \tau_i} \quad (i = 1, 2)$$

Where $R(t)$ is the intensity usually assumed to decay as the sum of individual exponential decays, A_i is the pre-exponential factor and τ_i is the decay time.

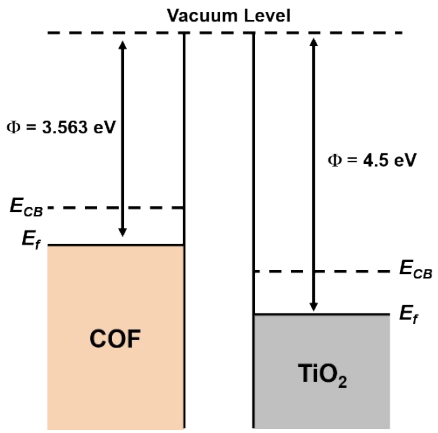

Fig. S15. Schematic representation of the work function of COF and TiO_2. The work function of COF is simulated to be 3.563 eV, and the work function of TiO_2 NTAs is 4.5 eV in literature.[8-10]

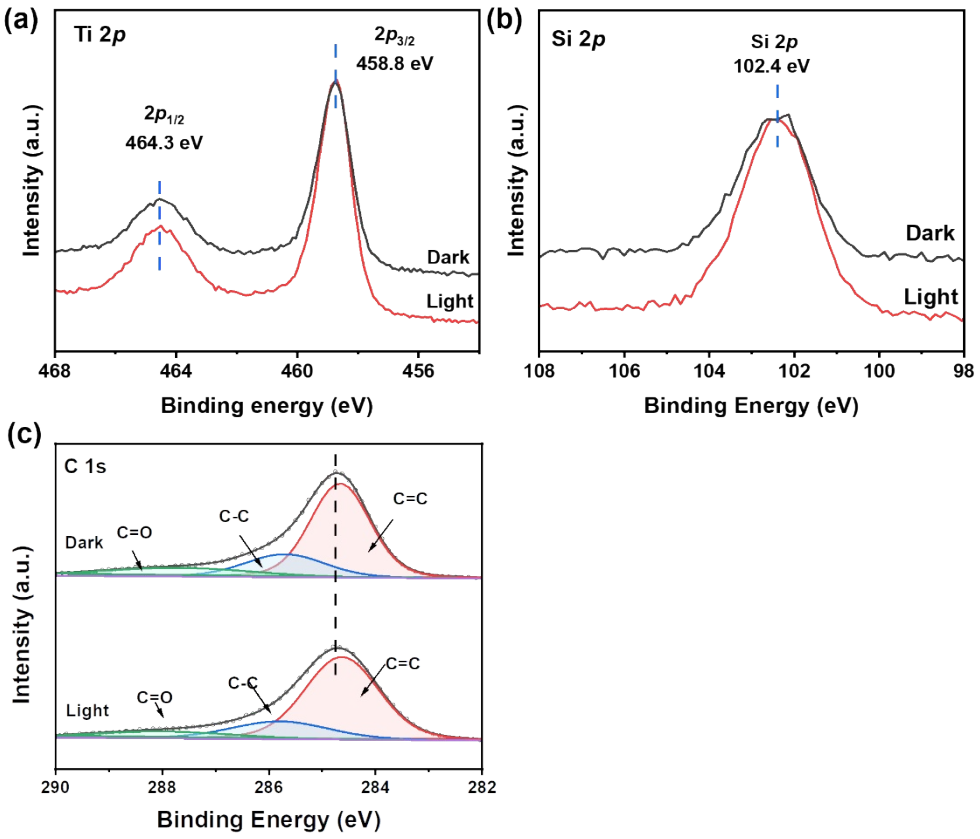

Fig. S16 In-situ irradiated X-ray photoelectron spectra (ISI-XPS) of (a) Ti *2p*, (b) Si *2p*, (c) C *1s*, compared to the spectra under dark conditions (top rows). No difference in the binding energy position for Ti *2p* spectra between ISI-XPS and XPS as the position is used for calibration.

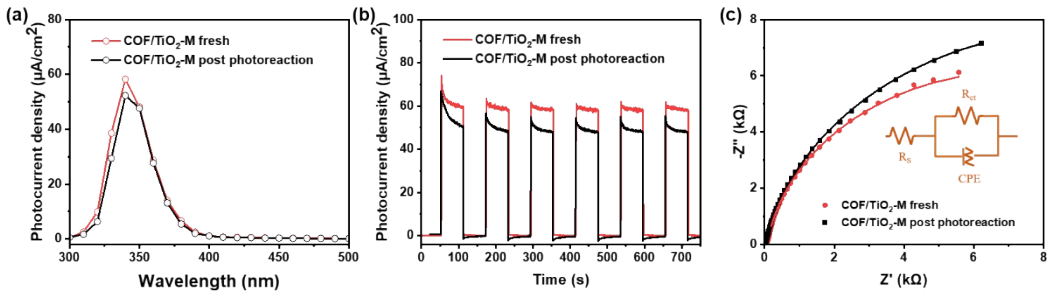

Fig. S17 (a) Photocurrent density, (b) photocurrent transient under 340 nm illumination, (c) electrochemical impedance spectra in Nyquist plots of COF/TiO_2-M as fresh sample and post photoreaction.

Table S8. The parameters used to fit the EIS on before and after photoreaction of COF/TiO_2-M. The Nyquist plot is shown in **Fig. S17**.

	R_{ct}/kΩ	R_s/Ω	CPE		χ^2
			Y_0	N	
Fresh	13.1	107.2	1.3×10^{-4}	0.94	0.0065
Post-photoreaction	16.3	59.4	1.9×10^{-4}	0.92	0.0054

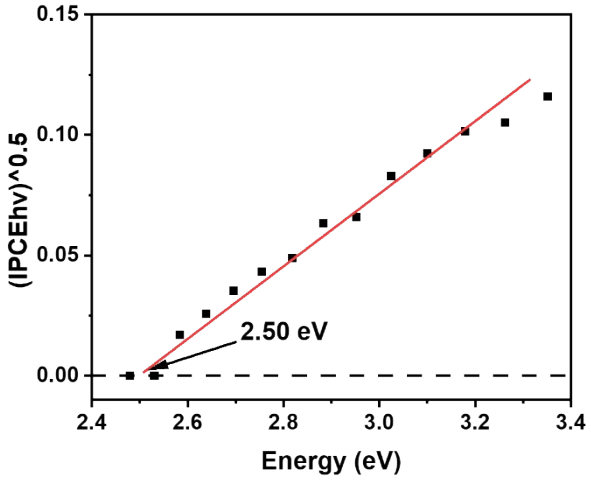

Fig. S18 Bandgap evaluation from photocurrent spectrum of COF.

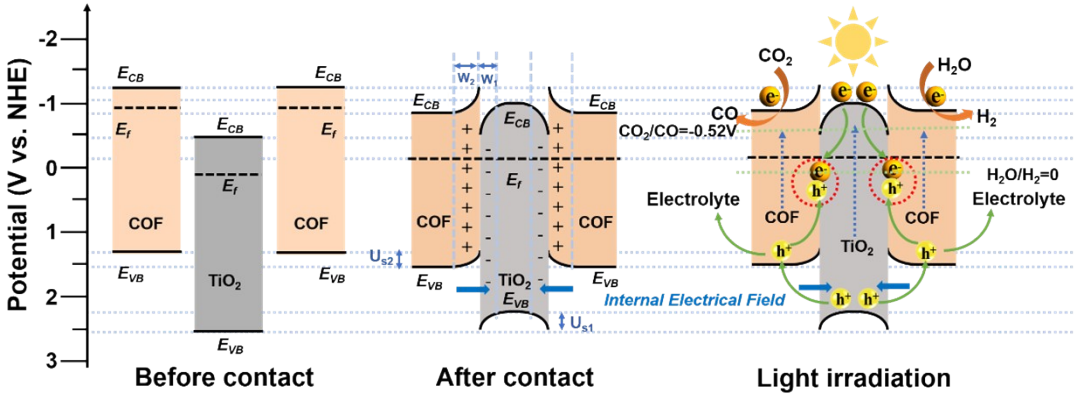

Fig. S19 Schematic diagram of energy band positions before contact, after contact, and under illumination.

With the thickening of W (width of space charge layer), the U_s increases, and the photogenerated electrons of TiO_2 combine with the holes generated by COF at the interface under illumination. The presence of COF thin film allows the transport of TiO_2 holes across the tube wall, instead, the thick film hinders the transport of carriers.

The specific value of W is quantified by the following equation:[11]

$$V_{BB} = \frac{qN_D W^2}{2\varepsilon\varepsilon_0}$$

Where V_{BB} is the energy band bending potential, determined by the difference between the Fermi levels of TiO_2 and COF, which is 1.3 V. The permittivity of anatase TiO_2 is 48, while that of organic polymers such as COF is reported to be about 1.6.[12]

References

1. W. Dong, Z. Qin, K. Wang, Y. Xiao, X. Liu, S. Ren and L. Li, *Angew. Chem. Int. Ed.*, 2023, **62**, e202216073.
2. X. Zhou, V. Häublein, N. Liu, N. T. Nguyen, E. M. Zolnhofer, H. Tsuchiya, M. S. Killian, K. Meyer, L. Frey and P. Schmuki, *Angew. Chem. Int. Ed.*, 2016, **55**, 3763-3767.
3. S. Yang, X. Feng, S. Ivanovici and K. Müllen, *Angew. Chem. Int. Ed.*, 2010, **49**, 8408-8411.
4. K. Gelderman, L. Lee and S. W. Donne, *J. Chem. Educ.*, 2007, **84**, 685.
5. X. Zhou, N. Liu and P. Schmuki, *ACS Catal.*, 2017, **7**, 3210-3235.
6. K. K. Manga, Y. Zhou, Y. Yan and K. P. Loh, *Adv. Funct. Mater.*, 2009, **19**, 3638-3643.
7. H. Shen, D. Shang, L. Li, D. Li and W. Shi, *Appl. Surf. Sci.* , 2022, **578**, 152024.
8. Y. Alivov, M. Klopfer and S. Molloi, *Appl. Phys. Lett.* , 2010, **96**, 243502.
9. Y. M. Kang, C. W. Wang, J. B. Chen, L. Q. Wang, D. S. Li, W. D. Zhu and F. Zhou, *J. Vac. Sci. Technol. B*, 2012, **30**, 041801.
10. G. Liu, F. Li, D. W. Wang, D.-M. Tang, C. Liu, X. Ma, G. Q. Lu and H.-M. Cheng, *Nanotechnology*, 2008, **19**, 025606.
11. Z. Zhang and J. T. Yates, Jr., *Chem. Rev.*, 2012, **112**, 5520-5551.
12. A. M. Evans, A. Giri, V. K. Sangwan, S. Xun, M. Bartnof, C. G. Torres-Castanedo, H. B. Balch, M. S. Rahn, N. P. Bradshaw, E. Vitaku, D. W. Burke, H. Li, M. J. Bedzyk, F. Wang, J. L. Brédas, J. A. Malen, A. J. H. McGaughey, M. C. Hersam, W. R. Dichtel and P. E. Hopkins, *Nat. Mater.*, 2021, **20**, 1142-1148.